

# HI Observations of Flat Galaxies

S. N. Mitronova<sup>1</sup>, W. K. Huchtmeier<sup>2</sup>, I. D. Karachentsev<sup>1</sup>, V. E. Karachentseva<sup>3</sup>, and Yu. N. Kudrya<sup>3</sup>

<sup>1</sup> *Special Astrophysical Observatory, Russian Academy of Sciences, Nizhnii Arkhyz, Karachai-Cherkessian Republic, 357147 Russia*

<sup>2</sup> *Max Planck Institut für Radioastronomie, Auf dem Hügel 69, D-53121 Bonn, Germany*

<sup>3</sup> *Astronomical Observatory, Kiev National University, Observatorna ul., Kiev, 304053 Ukraine*

## Abstract

We present the HI observations of 94 flat spiral galaxies from RFGC (the Revised Flat Galaxy Catalog) and 14 galaxies from 2MFGC (the 2MASS selected Flat Galaxy Catalog) performed with the 100-m radio telescope in Effelsberg (Germany). HI fluxes, heliocentric radial velocities, and HI line widths are given for 65 detected galaxies. We present a mosaic of HI profiles. We calculated some of the global parameters of the galaxies and analyzed the linear correlations between them. The ratios of the total (indicative) masses of the galaxies to their luminosities lie within the range 0.4 with a mean of 3.8 ( $M_{\odot}/L_{\odot}$ ), and the mean mass fraction of neutral hydrogen is 13%. Upper limits are given for the radio fluxes from 43 undetected galaxies.

**Key words:** galaxies, radio sources.

## INTRODUCTION

One of the central problems in extragalactic astronomy is to study the collective motions of galaxies by analyzing their peculiar velocities  $V_{pec} = V_{3K} - Hr$ . Here,  $V_{3K}$  is the measured radial velocity of the galaxy reduced to the frame of the 3K microwave background radiation (Kogut et al. 1993), and  $Hr$  is the distance to the galaxy (in  $\text{km s}^{-1}$ ) determined independently of its radial velocity. The main method of determining  $Hr$  for spiral galaxies is based on the Tully–Fisher (1977) relation between the absolute parameters of the galaxy (its luminosity and linear diameter) and the width of the 21-cm HI line. Karachentsev (1989) showed that the late-type edge-on spiral galaxies are appropriate objects for investigating the large-scale streams for several reasons: (1) the flat, disklike galaxies have a simple structure; (2) applying the simple selection criterion based on the apparent axial ratio  $a/b > 7$  to them yields a morphologically homogeneous sample; (3) the detection probability of such galaxies in the 21-cm line is very high; and (4) since the flat galaxies are located mostly outside groups and clusters, their structure remains undistorted and they are not affected by large virial motions. To compile our catalog of flat edge-on galaxies, we conducted an all-sky survey using blue and red POSS-I and ESO/SERC maps. FGC (the Flat Galaxy Catalog; Karachentsev et al. 1993) includes galaxies with apparent axial ratios  $a/b > 7$  and angular diameters  $a > 0.6'$ . The updated and supplemented version of this catalog, RFGC (the Revised Flat Galaxy Catalog; Karachentsev et al. 1999a), contains 4236 galaxies and is one of the best samples for studying the large-scale cosmic streams of galaxies (Karachentsev et al. 2000a; Kudrya et al. 2003), since it is highly homogeneous and has the required completeness (Kudrya et al. 1996, 1997; Feldman et al. 2003).

Extensive high-accuracy measurements of the radial velocities ( $V_h$ ) and HI-line widths ( $W$ ) are needed to use the Tully–Fisher (TF) relation. For this purpose, flat galaxies were observed with large radio telescopes: the 305-m radio telescope

in Arecibo (Giovanelli et al. 1997) and the 100-m radio telescope in Effelsberg (Huchtmeier et al. 2005). Makarov et al. (2001) measured the rotation curves of 300 flat galaxies with the 6-m telescope at the Special Astrophysical Observatory of the Russian Academy of Sciences. Based on original observations and published data, Karachentsev et al. (2000b) compiled a list of peculiar velocities for 1327 RFGC galaxies. The published homogeneous and complete near infrared all-sky survey, 2MASS (the Two Micron All-Sky Survey; Skrutskie et al. 1997), opened up new opportunities for studying the collective motions of galaxies based on the near-infrared TF relation (Karachentsev et al. 2002; Kudrya et al. 2003). 2MASS J-, H-, and K-band photometry is available for 71% of the RFGC galaxies, but the radial velocities and HI-line widths were reliably measured only for 25% of them. A program of HI observations of RFGC galaxies with the 100-m radio telescope in Effelsberg was initiated in 2001. Huchtmeier et al. (2005) published the first results of observations of 268 galaxies.

Analyzing the properties of RFGC galaxies in the near infrared (2MASS) and comparing them with optical data allowed the selection criteria to be developed for compiling a new catalog of flat galaxies based on 2MASS. The 2MFGC all-sky catalog of disklike galaxies (Mitronova et al. 2004) contains IR photometry and LEDA and NED identifications for 18020 objects with XSC 2MASS axial ratios  $a/b \geq 3$ .

In this paper, we present the observations of 94 RFGC galaxies and the test observations of 14 2MFGC galaxies performed with the 100-m radio telescope in the fall of 2004.

## HI OBSERVATIONS

The HI observations of RFGC galaxies have been performed with the 100-m radio telescope in Effelsberg (Germany) since October 2001. Using the optical and infrared parameters of flat galaxies, we estimated their expected radial velocities

and selected objects in the working range of the telescope  $V_h \leq 9500 \text{ km s}^{-1}$  for our observations. We also included in our observational application galaxies for which the radial velocities were known from optical observations with an accuracy lower than  $30 \text{ km s}^{-1}$  and no HI line width measurements were available. We also included in our list galaxies for which it was necessary to improve  $V_h$  and (or)  $W$ , since they deviated by more than  $3\sigma$  from the regression line in the TF relation or the magnitudes of their peculiar velocities were larger than  $3000 \text{ km s}^{-1}$ . The spectroscopic observations with the 100-m radio telescope were performed in full energy mode (ON-OFF), combining the measurements in the source's field with those in the comparison field whose location was earlier than the galaxy's location by 5 min in right ascension. The beam FWHM of the telescope at 21 cm is  $9.3'$ . The temperature of the system consisting of two receivers is  $30K$ . The 1024-channel autocorrelator was divided into four 256-channel bands shifted in frequency by 11 MHz. To cover the entire velocity range from 250 to  $9050 \text{ km s}^{-1}$ , we used 12.5-MHz-wide bands. In this case, the resulting resolution per channel is  $10.4 \text{ km s}^{-1}$ . For galaxies with known radial velocities, we used 6.25-MHz-wide bands, which provided a resolution of  $5.2 \text{ km s}^{-1}$  per channel. We used weighted (or equivalent) smoothing for most galaxies to improve the signal-to-noise ratio. From one to five scans were made for each galaxy; the total accumulation time was about  $2^h$  per galaxy.

## RESULTS OF THE OBSERVATIONS

Figures 1 and 2 show the HI profiles for the detected RFGC and 2MFGC galaxies. No HI line profiles are shown for two RFGC galaxies (2553 and 4160) with complex spectra.

Table 1 contains the results of our radio observations of 94 RFGC galaxies as well as cataloged (optical) data. The columns of this table give the following: (1) the RFGC galaxy number; (2) the J2000.0 equatorial coordinates; (3) the major and

minor diameters ( $a \times b$ ) in arcmin corresponding to the  $B$  band 25 mag arcsec $^{-2}$  isophote; (4) the total  $B$ -band magnitudes; (5) the morphological type in the Hubble system, where Sb = 3, Sc = 5, and Sd = 7; (6) the HI-line flux in Jy km s $^{-1}$  corrected for the ratio of the galaxy's angular diameter to the telescope's aperture; (7) the maximum flux and the rms noise error in mJy; (8) the mean heliocentric radial velocity and its error in km s $^{-1}$ ; (9–11) the HI line widths at 50%, 25%, and 20% of the peak flux level in km s $^{-1}$ . The colons (:) in the table mark unreliable measurements with low signal-to-noise ratios and a complex structure of the HI profiles.

Table 2 gives data for 2MFGC galaxies. The content of its columns corresponds to Table 1 with the following differences: (1) the galaxy names in known catalogs taken from the NED electronic database; (3) the major and minor diameters ( $a \times b$ ) in arcmin taken from the LEDA electronic database; and (4) the total  $B$ -band magnitudes taken from the LEDA database.

For 40 RFGC and three 2MFGC galaxies, we failed to find the HI line in the range of radial velocities under study. Tables 1 and 2 give only the rms noise errors for these galaxies. The undetected galaxies probably lie outside the working spectral range, although it may well be that the HI fluxes from some of the nearby early-type galaxies could be below the instrumental detection threshold.

## GLOBAL OPTICAL AND HI PARAMETERS OF GALAXIES

We calculated the global characteristics of 54 detected RFGC galaxies using the radio observations and optical parameters from Table 1. As the distance indicator, we used the radial velocity of the galaxy reduced to the centroid of the Local Group,

$$V_{LG} = V_h + V_a[\cos b \cdot \cos(b_a) \cdot \cos(l - l_a) + \sin b \cdot \sin(b_a)], \quad (1)$$

where  $l$  and  $b$  are the Galactic coordinates, and  $V_h$  is the measured heliocentric radial velocity; the apex parameters,  $V_a = 316$  km c $^{-1}$ ,  $l_a = 93^\circ$ ,  $b_a = -4^\circ$ , were

taken from the paper by Karachentsev and Makarov (1996). We calculated the HI mass as

$$\log(M_{HI}/M_{\odot}) = \log F + 2 \log(V_{LG}/H_0) + 5.37, \quad (2)$$

where the Hubble constant was assumed to be  $H_0 = 75 \text{ km s}^{-1} \text{ Mpc}^{-1}$ , and  $F$  is the detected 21-cm flux in  $\text{Jy km s}^{-1}$  corrected for the ratio of the galaxy's angular diameter to the telescope's aperture. We calculated the indicative mass of the galaxy within the standard optical diameter from the relation

$$\log(M_{25}/M_{\odot}) = 2 \log(W_c) + \log(a_c) + \log(V_{LG}/H_0) + 3.92, \quad (3)$$

where  $W_c$  is the hydrogen line width corrected for turbulence (Tully and Fouqué 1985) and relativistic broadening,  $W_c = W_{50}/(1 + V_h/c)$ . The angular diameter was reduced to the 25 mag arcsec<sup>-2</sup> isophote (Kudrya et al. 1997) and corrected for the Galactic absorption and the galaxy's tilt ( $\log a_c = \log a + 0.09A_B - 0.2 \log(a/b)$ ). To calculate the luminosity, we use the relation

$$\log(L/L_{\odot}) = 2 \log(V_{LG}/H_0) - 0.4(B_t - \Delta B) + 12.16, \quad (4)$$

where the total magnitude  $B_t$  was corrected for the absorption  $A_B$  (Schlegel et al. 1998) and the galaxy's tilt  $\Delta B = A_B + 1.2 \log(a/b)$ .

Table 3 gives the calculated global parameters. Its columns contain the following: (1) the RFGC galaxy number; (2) the radial velocity  $V_{LG}$  reduced to the centroid of the Local Group; (3) the HI line width  $W_c$  at 50% of the peak flux level corrected for turbulence and relativistic broadening; (4) the logarithm of the HI mass,  $\log(M_{HI}/M_{\odot})$ ; (5) the logarithm of the galaxy's indicative mass,  $\log(M_{25}/M_{\odot})$ ; (6) the logarithm of the galaxy's total luminosity,  $\log(L/L_{\odot})$ ; (7) the HI mass-to-luminosity ratio,  $M_{HI}/L$ ; (8) the galaxy's total mass-to-luminosity ratio,  $M_{25}/L$ . (the values in columns 4–8 are in solar units); and (9) the mass fraction of neutral hydrogen,  $M_{HI}/M_{25}$ .

According to Table 3, the mean depth of the sample is  $4823 \text{ km s}^{-1}$ , which corresponds to 64 Mpc. The total mass-to-luminosity ratios of the galaxies lie within the range 0.4–8.2 with a mean of 3.8, and the mass fraction of neutral hydrogen is 13%.

Karachentsev et al. (1999b) performed a statistical analysis of the global parameters for 587 flat spiral galaxies using the observations performed by Giovanelli et al. (1997) with the Arecibo radio telescope. Huchtmeier et al. (2005) presented the statistics of global parameters for 121 detected RFGC galaxies.

Table 4 gives the statistical characteristics of the distribution of 50 flat galaxies in integrated parameters. Comparison of the mean values of all parameters with those for the sample of 121 flat galaxies shows that they are almost equal.

In Figs 3 and 4, the logarithm of the HI mass-to-luminosity ratio and the logarithm of the indicative mass-to-luminosity ratio are plotted against radial velocity  $V_{LG}$  for flat galaxies. Since the radial velocity is a distance indicator, it can be noted that  $M_{HI}/L$  and  $M_{25}/L$  decrease with distance only slightly; i.e., there is virtually no distance selection effect. Arbitrarily oriented spiral galaxies are known to show no variation of  $M/L$  with distance either (Roberts and Haynes 1994).

Figure 5 shows the distribution of galaxies in morphological type. All of the 94 RFGC galaxies under study are shown on the histogram, and the types of 54 detected galaxies of them are marked by double hatching. Most of the objects belong to the morphological types *Sbc* – *Sd*, where the detection level is higher.

The data in Table 5 agree with the conclusions of our previous paper (Huchtmeier et al. 2005) that the mean values of the global parameters under consideration do not change within the error limits for galaxies of various morphological types. This conclusion is consistent with the HI observations of edge-on spiral galaxies (Karachentsev et al. 1999b) and arbitrarily oriented spirals of various types (Haynes and Giovanelli 1984) from the catalog of isolated galaxies by Karachentseva (1973).

## BIVARIATE DISTRIBUTIONS OF GLOBAL PARAMETERS

The correlations between global parameters lead us to important conclusions about the differences between the properties of the disk structures in giant and dwarf galaxies. The observed differences can characterize the different formation and equilibrium conditions for the gaseous disks and the inequality of the star formation rates and intensities in them. It is also assumed that the contribution of dark matter depends on the linear sizes of galaxies.

Figures 6 and 7 show the bivariate distributions of global parameters for 50 detected RFGC galaxies, and Table 6 lists the parameters of the linear regression  $y = kx + c$  for various relations. The logarithms of the various global parameters of flat galaxies are the variables  $x$  and  $y$ . Columns 4 and 5 give the correlation coefficients  $\rho(x, y)$  and the standard deviations  $\sigma(y)$ ; columns 6 and 7 contain the regression parameters  $k$  and  $c$  and their standard errors, respectively. Figure 6a and the first row of Table 6 show the relation between the logarithm of the HI mass (in  $M_\odot$ ) and the logarithm of the galaxy's linear diameter  $A_{25}$  (in kpc) calculated from the angular diameter  $a_c$  using the formula

$$A_{25} = 0.29 \cdot a_c \cdot V_{LG}/H_0. \quad (5)$$

The linear relation suggests that the HI density in the disks of spiral galaxies is virtually constant and does not depend on the linear size. The conditions for star formation in them appear to have been approximately identical in them. The statistically insignificant decrease in  $\log (M_{HI}/A_{25}^2)$  toward the massive galaxies (row 10 in Table 6) may be due to the internal absorption of the HI flux in the disks of the largest galaxies. Other parameters, the indicative mass and the total luminosity (see rows 2 and 3 in Table 6 and Fig. 6b), also correlate well with the linear diameter.

The dependences of the HI mass  $\log M_{HI}$  and the indicative mass  $\log M_{25}$  on the luminosity  $\log L$  show a systematic decrease in  $M/L$  from dwarf galaxies to giant



spirals (see Figs. 6c and 6d and rows 4 and 5 in Table 6). This is to be expected if the relative abundance of the dark matter in giant galaxies is lower than that in dwarf galaxies.

Since the width of the 21-cm HI line does not depend on the distance to the galaxy, taken as the argument for the bivariate distributions of global parameters, it allows the morphology and luminosity selection effects to be reduced. Figure 6e (row 6 in Table 6) shows the linear relation between the galaxy's size  $\log A_{25}$  (in kpc) and the amplitude of its internal rotation determined as the width of the 21-cm line. The slope of the linear regression in this Tully–Fisher (1977) relation is 1.28 with a standard deviation of 0.15. The correlations between  $\log(M_{25}/L)$  and  $\log(M_{HI}/L)$  and the 21-cm line width are also well defined; their parameters are listed in rows 7 and 8 of Table 6. We see from Fig. 6f (row 9 in Table 6) that the relative hydrogen abundance increases from giant galaxies to dwarf galaxies in the same way as for arbitrarily oriented spiral galaxies whose luminosities are not affected strongly by internal absorption (Huchtmeier and Richter 1988, Staveland-Smith and Davies 1988).

The relation between the logarithm of the HI mass,  $\log M_{HI}$ , and the specific angular momentum  $\log(A_{25}W_{50})$  (see Fig. 7 and row 11 in Table 6) has a high correlation coefficient; the slope of the linear regression is 1.19. Zasov (1974) pointed out that such a relation must hold in the gas-rich disks of spiral galaxies with active star formation. Karachentsev et al. (1999b) corroborated the linear relation between  $\log M_{HI}$  and  $\log(A_{25}W_{50})$  for flat galaxies and Zasov's conclusion that the gaseous disks of galaxies must be near the gravitational stability boundary irrespective of the linear sizes of the galaxies.

## ACKNOWLEDGMENTS

We are grateful to Max Planck Institut für Radioastronomie (Effelsberg, Germany) for the observational data obtained with the 100-m radio telescope. This work was supported by the Russian Foundation for Basic Research and Deutsche

Forschungsgemeinschaft (DFG) (grant no. 02-02-04012).

## REFERENCES

1. H. Feldman, R. Yuzhkievich, M. Davis, et al., *Astrophys. J.* 596, L131 (2003).
2. R. Giovanelli, E. Avera, and I. D. Karachentsev, *Astron. J.* 114, 122 (1997).
3. M. P. Haynes and R. Giovanelli, *Astron. J.* 89, 758 (1984).
4. W. K. Huchtmeier, Yu. N. Kudrya, I. D. Karachentsev, et al., *Astron. Astrophys.* (2005) (in press).
5. W. K. Huchtmeier and O. G. Richter, *Astron. Astrophys.* 203, 237 (1988).
6. I. D. Karachentsev, *Astron. J.* 97, 1566 (1989).
7. I. D. Karachentsev et al., *Astron. Astrophys.* (2004) (in press).
8. I. D. Karachentsev, V. E. Karachentseva, Yu. N. Kudrya, et al., *Bull. Spec. Astron. Obs. Russ. Acad. Sci.* 47, 5 (1999).
9. I. D. Karachentsev, V. E. Karachentseva, and Yu. N. Kudrya, *Pis'ma Astron. Zh.* 25, 3 (1999b) [*Astron. Lett.* 25, 1 (1999b)].
10. I. D. Karachentsev, V. E. Karachentseva, Yu. N. Kudrya, et al., *Astron. Zh.* 77, 175 (2000a) [*Astron. Rep.* 33, 150 (2000a)].
11. I. D. Karachentsev, V. E. Karachentseva, Yu. N. Kudrya, et al., *Bull. Spec. Astron. Obs. Russ. Acad. Sci.* 50, 5 (2000b).
12. I. D. Karachentsev, V. E. Karachentseva, and S. L. Parnovskii, *Astron. Nachr.* 314, 97 (1993).
13. I. D. Karachentsev and D. I. Makarov, *Astron. J.* 111, 535 (1996).
14. I. D. Karachentsev, S. N. Mitronova, V. E. Karachentseva, *Astron. Astrophys.* 396, 431 (2002).
15. V. E. Karachentseva, *Soobshch. Spets. Astron. Obs. Akad. Nauk SSSR* 8, 3 (1973).
16. A. Kogut, C. Lineweaver, G.F. Smoot, et al., *Astrophys. J.* 419, 1 (1993).

17. Yu. N. Kudrya, I. D. Karachentsev, V. E. Karachentseva, and S. L. Parnovskii, *Pis'ma Astron. Zh.* 22, 330 (1996) [*Astron. Lett.* 22, 295 (1996)].
18. Yu. N. Kudrya, I. D. Karachentsev, V. E. Karachentseva, and S. L. Parnovskii, *Pis'ma Astron. Zh.* 23, 730 (1997) [*Astron. Lett.* 23, 652 (1997)].
19. Yu. N. Kudrya, V. E. Karachentseva, I. D. Karachentsev, et al., *Astron. Astrophys.* 407, 889 (2003).
20. S. N. Mitronova, I. D. Karachentsev, V. E. Karachentseva, et al., *Bull. Spec. Astron. Obs. Russ. Acad. Sci.* 57, 5 (2004).
21. M. S. Roberts and M. P. Haynes, *Ann. Rev. Astron. Astrophys.* 32, 115 (1994).
22. D. J. Schlegel, D. P. Finkbeiner, and M. Davis, *Astrophys. J.* 500, 525 (1998).
23. M. F. Skrutskie, S. E. Schneider, R. Stiening, et al., in *The Impact of Large Scale Near-IR Sky Surveys* Ed. by F. Garzon et al., (Kluwer, Dordrecht, 1997), Vol. 210, p. 25.
24. L. Staveland-Smith and R.D. Davies, *Mon. Not. Roy. Astron. Soc.* 231, 833 (1988).
25. R. B. Tully and J. R. Fisher, *Astron. Astrophys.* 54, 661 (1977).
26. R. B. Tully and P. Fouqué, *Astrophys. J., Suppl. Ser.* 58, 67 (1985).
27. A. V. Zasov, *Astron. Zh.* 51, 1225 (1974) [*Sov. Astron.* 18, 730 (1974)].

Table 1: Results of the HI observations of RFGC galaxies with the 100-m radio telescope

RFGC	RA(2000)DEC	$a \times b$	$B_t$	$T$	$F$	$S_{max}$	$V_h$	$W_{50}$	$W_{25}$	$W_{20}$
1	2	3	4	5	6	7	8	9	10	11
161	004215.1–180940	$3.36 \times .30$	14.5	7	19.1	$139 \pm 4$	$1553 \pm 2$	192	205	208
208	005332.6+025527	$1.71 \times .21$	15.4	6	4.2	$\pm 4$	$4843 \pm 3$	250		
280	011406.7+380723	$1.16 \times .16$	16.0	5		$\pm 2$				
329	012737.1+510851	$0.87 \times .11$	18.1	6	2.1	$23 \pm 2$	$6096 \pm 11$	129		
411	015616.1–225404	$2.23 \times .27$	14.9	3	8.5	$68 \pm 9$	$1828 \pm 1$	229	240	
458	020715.4+461520	$1.12 \times .13$	16.4	7		$\pm 5$				
492	021732.5–113108	$1.22 \times .17$	15.8	8	3.6	$32 \pm 4$	$3957 \pm 4$	210		
493	021735.9–214554	$0.95 \times .09$	16.6	6	4.1	$26 \pm 4$	$6423 \pm 4$	264		
544	023052.8+432100	$1.27 \times .11$	16.2	4	0.5:	$\pm 3$	6100:			
620	025426.6+423900	$2.43 \times .15$	15.4	7	8.8	$68 \pm 6$	$2167 \pm 2$	203	213	
668	030854.8+703349	$1.68 \times .24$	17.0	3	1.3	$37 \pm 9$	$4330 \pm 5$			
734	032846.7+363323	$1.79 \times .20$	16.5	4	5.4	$41 \pm 6$	$4701 \pm 4$	129	157	
860	043018.5+884616	$1.10 \times .13$	16.3	6		$\pm 4$				
914	045213.2–182335	$1.53 \times .16$	15.7	6	1.4	$18 \pm 4$	$9573 \pm 5$	415		
974	052320.9+854023	$0.83 \times .09$	16.9	5		$\pm 6$				
982	052644.4–191236	$1.39 \times .19$	15.8	5	7.6	$30 \pm 6$	$8336 \pm 3$	512		
987	053012.0+555216	$1.57 \times .21$	18.0	9	9.5	$60 \pm 3$	$2182 \pm 4$	187	210	214
1053	061021.8+504706	$1.38 \times .17$	15.8	4	3.3	$27 \pm 4$	$7775 \pm 5$	420		
1063	061318.7+530643	$1.19 \times .16$	16.2	7		$\pm 4$				
1064	061342.3+810425	$2.04 \times .24$	15.6	4	3.2	$28 \pm 4$	$4266 \pm 7$	176		
1119	063900.2+572258	$1.00 \times .12$	16.4	5		$\pm 5$				
1185	071554.5+675902	$2.02 \times .22$	15.3	5	4.7	$40 \pm 3$	$1153 \pm 3$	172	183	
1207	072225.0+491642	$0.84 \times .11$	16.4	9		$\pm 4$				
1280	075507.0+425728	$0.78 \times .09$	16.8	6	2.2	$15 \pm 4$	$7490 \pm 5$	280		
1282	075524.7+561002	$0.96 \times .11$	16.7	5		$\pm 4$				
1300	080009.6+562154	$2.33 \times .22$	15.1	5	5.0	$20 \pm 3$	$9095 \pm 5$	629		
1340	081359.5+454434	$5.17 \times .58$	13.6	6	43.9	$322 \pm 3$	$559 \pm 1$	170	189	194
1351	081709.6+560249	$0.68 \times .09$	16.9	6		$\pm 4$				
1405	083812.0+455255	$0.87 \times .10$	16.5	6	1.7	$16 \pm 3$	$7070 \pm 7$	264		
1425	084421.6+093215	$1.23 \times .10$	16.4	6	4.0	$26 \pm 6$	$4064 \pm 5$	226		
1451	085419.0+542728	$0.90 \times .11$	16.5	6	2.1	$10 \pm 3$	$7449 \pm 5$	350		
1490	090738.9+283808	$1.10 \times .10$	16.4	7	1.0	$9 \pm 2$	$6682 \pm 14$	265		
1524	091831.0+493244	$1.18 \times .15$	16.0	6		$\pm 11$				
1537	092145.1+641528	$4.31 \times .53$	13.9	5	49.8	$209 \pm 4$	$1574 \pm 2$	308	336	341
1543	092311.8–265631	$1.56 \times .17$	15.8	5	8:	$70 \pm 11$	$2410 \pm 3$	193		
1566	093140.8–160231	$1.84 \times .21$	15.3	7		$\pm 1$				
1583	093555.0+480848	$1.57 \times .22$	15.6	4		$\pm 13$				

1	2	3	4	5	6	7	8	9	10	11
1612	094402.4+682212	$0.74 \times .09$	16.8	6		$\pm 5$				
1626	094650.4+794839	$2.49 \times .22$	15.1	6	11.3	$86 \pm 3$	$1540 \pm 2$	170	183	186
1711	100439.1+602759	$0.88 \times .10$	16.6	6	1.7	$16 \pm 2$	$2216 \pm 10$	144		
1735	101001.0+715221	$0.88 \times .10$	16.6	6	1.8	$19 \pm 3$	$6327 \pm 5$	189		
1893	105124.0-195324	$4.26 \times .48$	14.0	6	13.4	$86 \pm 13$	$2067 \pm 1$	229		
1897	105236.0+394814	$0.68 \times .08$	17.0	5		$\pm 5$				
1940	110157.1+470540	$1.88 \times .15$	15.8	5	3.4	$19 \pm 3$	$6583 \pm 5$	378		
1988	111327.8+072553	$0.73 \times .09$	16.7	6		$\pm 8$				
2056	113057.6-040507	$0.92 \times .10$	16.7	7		$\pm 5$				
2093	114227.4+513551	$3.70 \times .45$	14.1	6	9.3	$73 \pm 3$	$975 \pm 2$	178	190	193
2116	114836.0+434316	$1.87 \times .20$	15.4	6	2.8	$27 \pm 4$	$735 \pm 5$	115		
2258	122016.6+480811	$1.20 \times .17$	15.8	9	1.7	$\pm 3$	$839 \pm 4$	122		
2296	122859.3+285143	$1.12 \times .15$	16.1	5	2.0	$17 \pm 3$	$8024 \pm 9$	435		
2298	122908.6+575454	$1.34 \times .16$	15.9	7	5.2	$46 \pm 7$	$799 \pm 4$	126	139	143
2335	123621.1+255906	$15.90 \times 1.85$	10.6	4	161	$420 \pm 5$	$1226 \pm 1$	506	521	524
2354	124128.8-031514	$0.67 \times .09$	17.1	8	1.3	$15 \pm 3$	$1803 \pm 6$	125		
2390	125105.0-082623	$1.12 \times .16$	16.1	6		$\pm 6$				
2437	130106.7-032235	$0.83 \times .11$	16.8	7	2.4	$23 \pm 5$	$2900 \pm 6$	156	175	
2443	130207.9+584159	$3.92 \times .32$	14.5	6		$\pm 3$				
2460	130514.9-002230	$1.09 \times .13$	16.3	7		$\pm 3$				
2463	130548.0+462743	$1.37 \times .19$	15.7	4		$\pm 3$				
2553	132409.6-175407	$1.25 \times .10$	16.4	7	1.9	$26 \pm 6$	$6994 \pm 15$	200		
2559	132525.7+044600	$1.01 \times .10$	16.7	5		$\pm 8$				
2574	132820.2-114703	$1.85 \times .24$	15.4	4		$\pm 3$				
2592	133341.5-111418	$0.99 \times .07$	17.0	7		$\pm 4$				
2626	134043.3-173314	$0.65 \times .07$	17.2	8		$\pm 7$				
2707	140425.4-002725	$0.90 \times .10$	16.6	7	1.5	$13 \pm 2$	$7380 \pm 6$	301		
2713	140621.6-054313	$1.28 \times .17$	15.8	4		$\pm 4$				
2737	141312.0-072648	$0.67 \times .08$	17.3	9		$\pm 6$				
2754	141741.0-052748	$1.29 \times .17$	15.9	5	6.1	$36 \pm 9$	$7057 \pm 5$	308		
2757	141833.6-050913	$1.15 \times .10$	16.4	7	3.2	$22 \pm 5$	$7010 \pm 11$	229		
2786	143007.2-062543	$1.46 \times .17$	15.9	4		$\pm 4$				
2856	144457.6+405234	$1.12 \times .16$	15.9	6	1.8	$14 \pm 3$	$5640 \pm 12$	216		
2902	150032.6+491027	$0.76 \times .10$	16.7	4		$\pm 4$				
2915	150438.9-181337	$0.84 \times .09$	16.9	7		$\pm 7$				
2943	151543.2-002524	$0.67 \times .09$	17.0	7		$\pm 5$				
2944	151543.2-102750	$0.83 \times .09$	16.8	7		$\pm 6$				

1	2	3	4	5	6	7	8	9	10	11
2955	151836.7−011101	$1.04 \times .11$	16.8	6		$\pm 6$				
2978	152628.8+411731	$2.26 \times .24$	15.1	5	5.6	$37 \pm 5$	$2481 \pm 1$	189		
3001	153443.0+082003	$1.48 \times .12$	16.3	6	2.6	$20 \pm 3$	$5803 \pm 4$	278		
3007	153654.0+511720	$1.10 \times .11$	16.4	5	4.2	$30 \pm 4$	$5847 \pm 5$	209		
3154	163231.2+674449	$1.12 \times .12$	16.4	4	4.0	$21 \pm 3$	$3423 \pm 4$	255		
3202	165140.3+532422	$0.68 \times .09$	16.8	8		$\pm 4$				
3210	165450.4+702617	$1.37 \times .19$	15.7	5		$\pm 3$				
3228	170247.8+444731	$0.65 \times .08$	17.3	8		$\pm 4$				
3230	170338.9+454832	$0.83 \times .10$	16.9	7		$\pm 5$				
3248	171145.3−254451	$0.98 \times .10$	16.7	5	3.4	$17 \pm 4$	$6330 \pm 6$	353		
3249	171149.2+473937	$0.85 \times .10$	16.7	6	2.5	$15 \pm 2$	$8320 \pm 15$	248		
3297	173721.6+602537	$1.12 \times .11$	16.4	5	2.5	$22 \pm 12$	$6220 \pm 6$	254		
3310	174810.8+530908	$0.95 \times .10$	16.5	6	1.5	$20 \pm 3$	$6744 \pm 9$	241		
3333	180645.1+874835	$1.77 \times .21$	15.6	4		$\pm 8$				
3377	183312.7+525655	$1.34 \times .11$	16.3	4	4.7	$25 \pm 6$	8418:			
3680	210236.0−134753	$1.68 \times .20$	15.6	3		$\pm 2$				
3870	220604.3−261107	$1.27 \times .13$	16.1	6		$\pm 2$				
4160	233900.0+493531	$0.83 \times .10$	16.7	6	1.2	$14 \pm 3$	$9319 \pm 10$			
4181	234438.4−273936	$1.14 \times .16$	16.1	5		$\pm 4$				
4214	235321.6+860141	$0.96 \times .09$	16.7	6	2.2	$12 \pm 3$	$5739 \pm 10$	361		

Table 2: Results of the HI observations of 2MFGC galaxies with the 100-m radio telescope

Name	RA(2000)DEC	$a \times b$	$B_t$	$T$	$F$	$S_{max}$	$V_h$	$W_{50}$	$W_{25}$	$W_{20}$
1	2	3	4	5	6	7	8	9	10	11
UGC256	002656.6+500150.7	$1.55 \times .29$	15.28	4	1.5	$11 \pm 3$				
UGC1928	022811.2+435109.7	$1.36 \times .30$	16.47	5	2.6	$16 \pm 3$	$6561 \pm 7$	432		
UGC69A	032702.2+725038.3	$2.10 \times .49$		3	17.7	$83 \pm 4$	$2074 \pm 3$	243	257	262
UGC2736	032627.6+403028.5	$1.57 \times .31$	14.64	2		$\pm 5$				
MCG-03-13-016	045013.7−171557.8	$1.83 \times .53$	14.25	4	5.2	$22 \pm 3$	$9248 \pm 8$	608		
UGC3127	044025.9−020112.6	$2.10 \times .42$	14.94	7	11.0	$74 \pm 5$	$3345 \pm 4$	192	205	209
UGC3342	054429.7+691756.3	$1.74 \times .39$	14.99	5	4.4	$31 \pm 4$	$3890 \pm 4$	294		
IRAS05442+46	054809.6+461531.0	$0.77 \times .60$	16.23	5	3.2	$27 \pm 4$	$6083 \pm 7$	190		
UGC4258	081047.6+465445.7	$1.43 \times .38$	18.16	6	5.3	$37 \pm 5$	$3124 \pm 4$	208	222	
UGC6390	112242.0+640358.7	$2.07 \times .30$	19.22	6	9.3	$91 \pm 4$	$982 \pm 3$	163	177	180
UGC6575	113626.5+581122.0	$1.88 \times .44$	14.57	5	14.6	$89 \pm 3$	$1216 \pm 5$	206	222	
UGC6894	115524.4+543926.3	$1.45 \times .25$	15.28	5	4.0	$39 \pm 5$	$850 \pm 4$	128		
NGC6244	164803.9+621201.6	$1.54 \times .32$	14.45	1		$\pm 4$				
UGC10713	170433.9+722647.5	$1.83 \times .32$	13.97	3	12.7	$89 \pm 4$	$1072 \pm 2$	230	242	244

Table 3: Optical and HI parameters of galaxies

RFGC	$V_{LG}$	$W_c$	$\log(M_{HI}/M_\odot)$	$\log(M_{25}/M_\odot)$	$\log(L/L_\odot)$	$M_{HI}/L$	$M_{25}/L$	$M_{HI}/M_{25}$
1	2	3	4	5	6	7	8	9
161	1623	191	9.3	10.1	9.6	0.57	3.76	0.15
208	4998	246	9.6	10.6	10.1	0.33	2.89	0.11
329	6352	126	9.5	9.9	10.3	0.20	0.48	0.42
411	1824	228	9.1	10.2	9.4	0.43	5.68	0.08
492	3985	207	9.4	10.2	9.8	0.42	2.83	0.15
493	6407	258	9.8	10.5	9.9	0.87	3.55	0.25
620	2357	202	9.3	10.2	9.7	0.36	2.89	0.13
734	4850	127	9.7	10.1	10.5	0.16	0.39	0.41
914	9438	402	9.7	11.2	10.6	0.12	4.06	0.03
982	8170	498	10.3	11.3	10.4	0.79	8.23	0.10
987	2321	186	9.3	10.2	10.3	0.11	0.79	0.14
1053	7874	409	9.9	11.2	10.7	0.19	3.48	0.05
1064	4476	174	9.4	10.3	10.2	0.16	1.31	0.12
1185	1305	171	8.5	9.8	9.1	0.29	5.00	0.06
1280	7509	273	9.7	10.5	10.0	0.56	3.56	0.16
1300	9182	610	10.2	11.8	10.9	0.25	8.02	0.03
1340	588	170	8.8	9.8	9.0	0.57	5.85	0.10
1405	7095	258	9.6	10.5	10.0	0.35	2.96	0.12
1425	3898	223	9.4	10.2	9.7	0.55	3.65	0.15
1451	7517	342	9.7	10.8	10.0	0.45	5.35	0.08
1490	6608	259	9.3	10.5	10.0	0.17	3.17	0.05
1537	1692	306	9.8	10.7	9.8	0.85	7.54	0.11
1543	2114	191	9.2	10.0	9.4	0.62	3.95	0.16
1626	1732	169	9.2	9.9	9.4	0.58	3.50	0.16
1711	2314	143	8.6	9.5	9.0	0.40	3.22	0.13
1735	6483	185	9.5	10.2	9.9	0.36	1.69	0.21
1893	1796	227	9.3	10.5	9.8	0.26	4.23	0.06
1940	6617	370	9.8	11.1	10.3	0.32	5.97	0.05
2093	1043	177	8.6	10.0	9.3	0.23	4.81	0.05
2116	765	115	7.8	9.1	8.5	0.21	4.14	0.05
2258	903	122	7.8	9.1	8.4	0.22	4.53	0.05
2296	7997	424	9.7	11.1	10.2	0.31	7.09	0.04
2298	912	126	8.3	9.2	8.4	0.67	5.21	0.13
2335	1189	504	10.0	11.5	10.8	0.15	5.65	0.03
2354	1639	124	8.2	9.1	8.5	0.50	4.42	0.11
2437	2749	155	8.9	9.6	9.0	0.69	3.79	0.18
2553	6807	195	9.6	10.4	10.2	0.23	1.47	0.15

RFGC	$V_{LG}$	$W_c$	$\log(M_{HI}/M_\odot)$	$\log(M_{25}/M_\odot)$	$\log(L/L_\odot)$	$M_{HI}/L$	$M_{25}/L$	$M_{HI}/M_{25}$
1	2	3	4	5	6	7	8	9
2707	7290	294	9.5	10.6	10.0	0.30	3.85	0.08
2754	6959	301	10.1	10.8	10.2	0.74	3.73	0.20
2757	6914	224	9.8	10.4	10.1	0.49	2.18	0.23
2856	5753	212	9.4	10.3	10.0	0.25	2.21	0.11
2978	2625	187	9.2	10.2	9.7	0.31	2.88	0.11
3001	5831	273	9.6	10.7	10.0	0.35	4.24	0.08
3007	6027	205	9.8	10.3	9.9	0.77	2.41	0.32
3154	3657	252	9.3	10.3	9.5	0.70	5.96	0.12
3248	6302	346	9.7	10.9	10.7	0.11	1.77	0.06
3249	8548	241	9.9	10.5	10.1	0.59	2.47	0.24
3297	6474	249	9.6	10.5	10.0	0.39	2.94	0.13
3310	6998	236	9.5	10.4	10.0	0.29	2.52	0.11
4214	5985	354	9.5	10.8	10.1	0.26	4.70	0.06

Table 4: Characteristics of the distributions of flat galaxies in integrated parameters

Parameter	Mean	Standard deviation	Skewness	Kurtosis
$\log(W_{50})$	2.36	0.17	0.33	-0.40
$\log(A_{25})$	1.17	0.29	-0.79	0.50
$\log(L_B)$	9.79	0.59	-0.65	0.01
$\log(M_{HI})$	9.38	0.56	-1.10	0.94
$\log(M_{25})$	10.35	0.59	-0.11	0.10
$\log(M_{HI}/L_B)$	-0.42	0.23	-0.16	-0.77
$\log(M_{HI}/A_{25}^2)$	7.03	0.23	-0.20	-0.82
$\log(M_{25}/L_B)$	0.56	0.21	-0.43	0.07
$\log(M_{HI}/M_{25})$	-0.98	0.28	-0.07	-0.42
$\log(A_{25} \cdot W_{50})$	3.53	0.43	-0.37	0.31

Table 5: Distribution of the mean parameters in morphological type for RFGC galaxies

N	Type	$\log(M_{HI}/A_{25}^2)$	$\log(M_{25}/L_B)$	$\log(M_{HI}/M_{25})$	$\log(M_{HI}/L_B)$
18	Sb,bc,c	$7.01 \pm 0.06$	$0.60 \pm 0.06$	$-1.03 \pm 0.08$	$-0.43 \pm 0.06$
20	Scd	$7.03 \pm 0.06$	$0.53 \pm 0.03$	$-0.96 \pm 0.06$	$-0.43 \pm 0.05$
12	Sd,dm,m	$7.07 \pm 0.05$	$0.55 \pm 0.05$	$-0.93 \pm 0.06$	$-0.38 \pm 0.07$



Table 6: Parameters of the linear regression  $y = kx + c$  for the global characteristics of RFGC galaxies

$N$	$y$	$x$	$\rho(xy)$	$\sigma(y)$	$k \pm \sigma_k$	$c \pm \sigma_c$
1	$\log(M_{HI})$	$\log(A_{25})$	0.92	0.22	$1.80 \pm 0.11$	$7.26 \pm 0.13$
2	$\log(M_{25})$	$\log(A_{25})$	0.93	0.22	$1.92 \pm 0.11$	$8.10 \pm 0.13$
3	$\log(L_B)$	$\log(A_{25})$	0.97	0.15	$2.00 \pm 0.08$	$7.45 \pm 0.09$
4	$\log(M_{HI})$	$\log(L_B)$	0.92	0.22	$0.87 \pm 0.05$	$0.81 \pm 0.52$
5	$\log(M_{25})$	$\log(L_B)$	0.94	0.20	$0.94 \pm 0.05$	$1.14 \pm 0.48$
6	$\log(A_{25})$	$\log(W_{50})$	0.77	0.19	$1.28 \pm 0.15$	$-1.86 \pm 0.37$
7	$\log(M_{25}/L_B)$	$\log(W_{50})$	0.39	0.19	$0.47 \pm 0.16$	$-0.54 \pm 0.38$
8	$\log(M_{HI}/L_B)$	$\log(W_{50})$	-0.24	0.23	$-0.32 \pm 0.19$	$0.34 \pm 0.45$
9	$\log(M_{25}/M_{HI})$	$\log(W_{50})$	-0.49	0.24	$-0.79 \pm 0.20$	$0.88 \pm 0.48$
10	$\log(M_{HI}/A_{25}^2)$	$\log(W_{50})$	-0.05	0.23	$-0.07 \pm 0.19$	$7.19 \pm 0.45$
11	$\log(M_{HI})$	$\log(A_{25} \cdot W_{50})$	0.91	0.23	$1.19 \pm 0.08$	$5.19 \pm 0.27$
12	$\log(M_{HI})$	$\log(W_{50})$	0.76	0.37	$2.49 \pm 0.31$	$3.48 \pm 0.73$
13	$\log(M_{25}/L_B)$	$\log(V_{LG})$	-0.32	0.20	$-0.20 \pm 0.08$	$1.25 \pm 0.30$

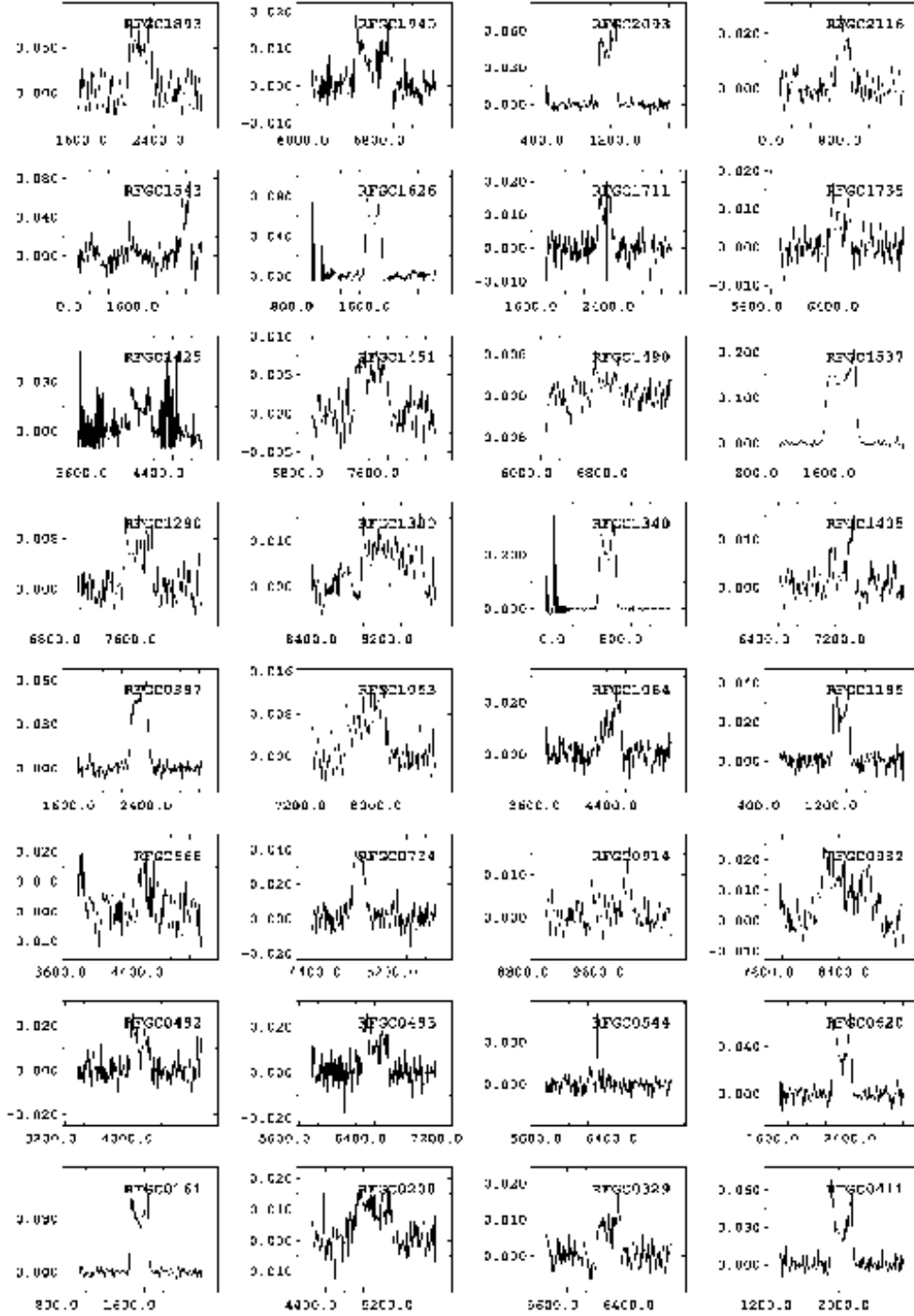


Figure 1: HI profiles for 51 RFGC galaxies from Table 1

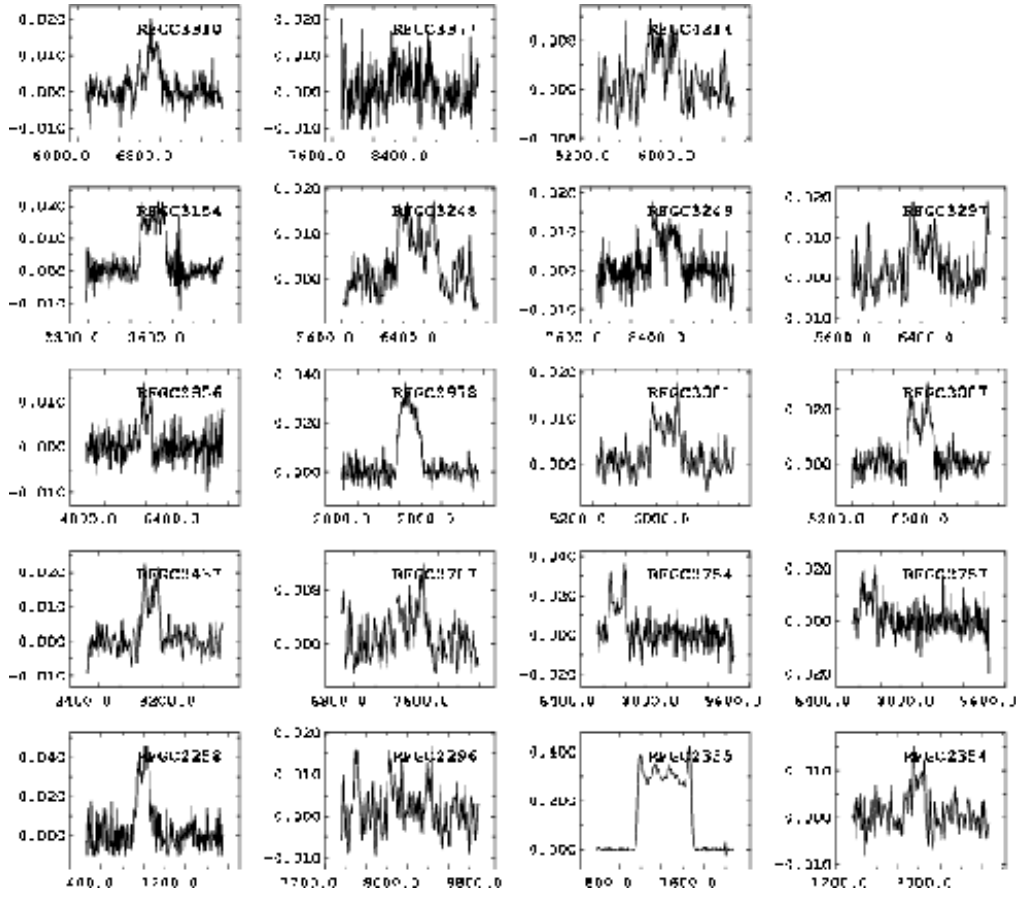


Figure 1: Contd.

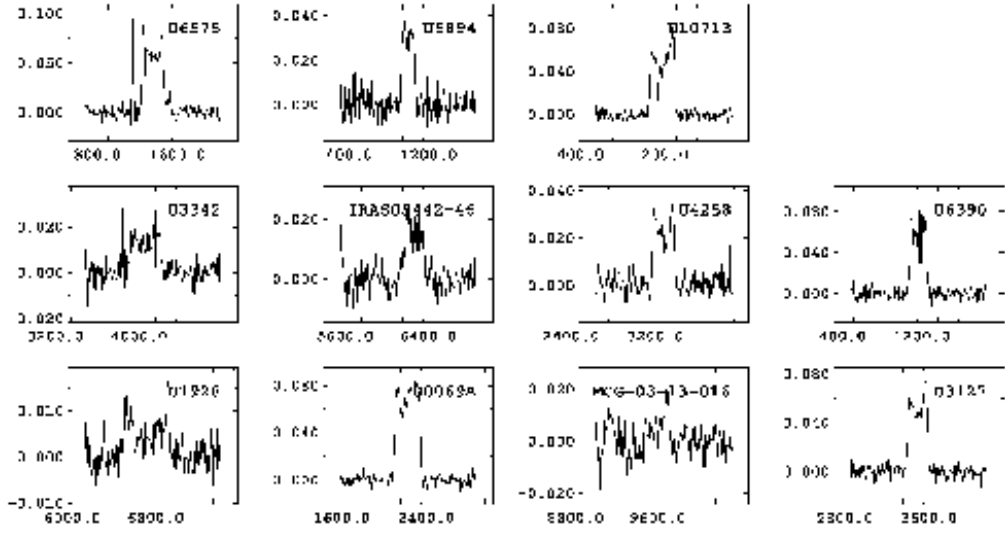


Figure 2: HI profiles for 11 2MFGC galaxies from Table 2

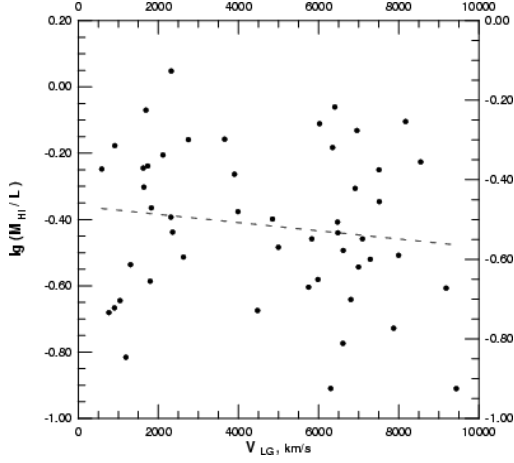


Рис.3

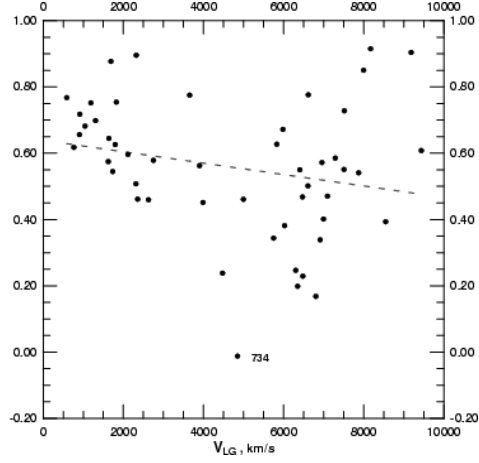


Рис.4

Figure 3: HI mass-to-luminosity ratio (in solar units) versus radial velocity (in  $\text{km s}^{-1}$ )

Figure 4: Total mass-to-luminosity ratio (in solar units) versus radial velocity (in  $\text{km s}^{-1}$ )

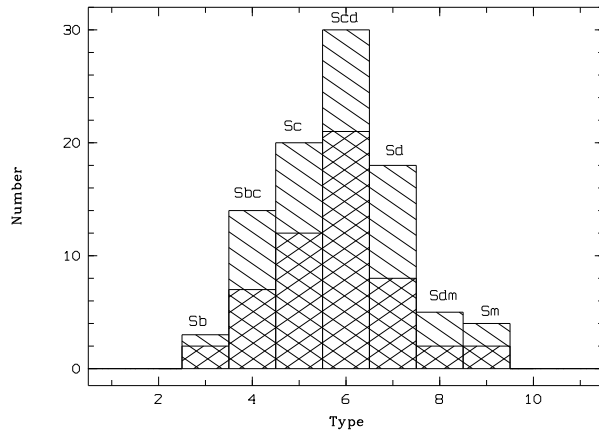


Figure 5: Distribution of galaxies in morphological type

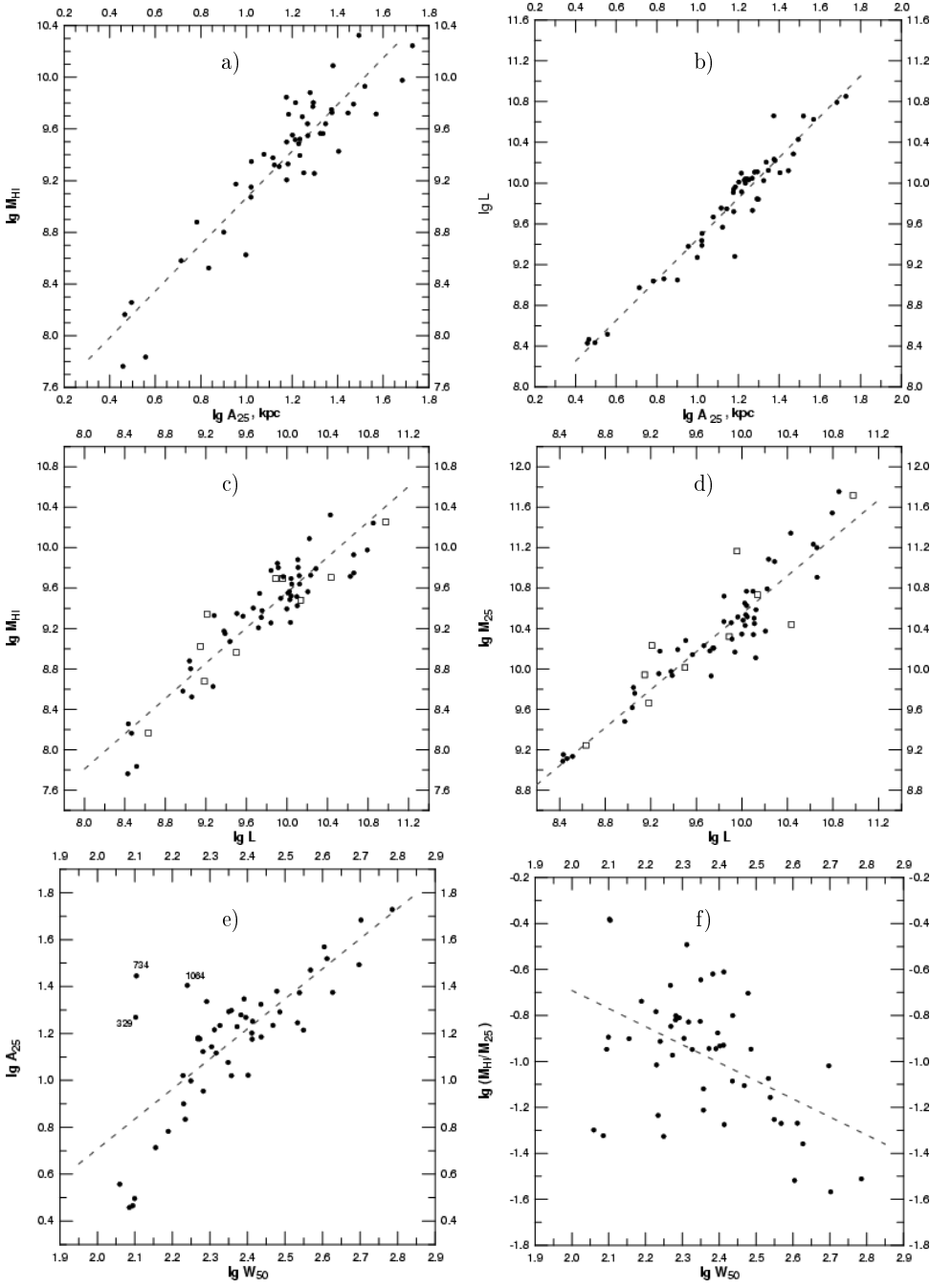


Figure 6: Bivariate relations between the global parameters reduced to solar units: (a) logarithm of the HI mass versus linear diameter (in kpc); (b) luminosity versus linear diameter; (c) HI mass versus luminosity; (d) indicative mass versus luminosity, the squares mark the 2MFGC galaxies; (e) linear diameter of the galaxy versus HI line width (in  $\text{km s}^{-1}$ ); and (f) HI mass fraction in the galaxy versus HI line width. The dashes represent the regression lines.

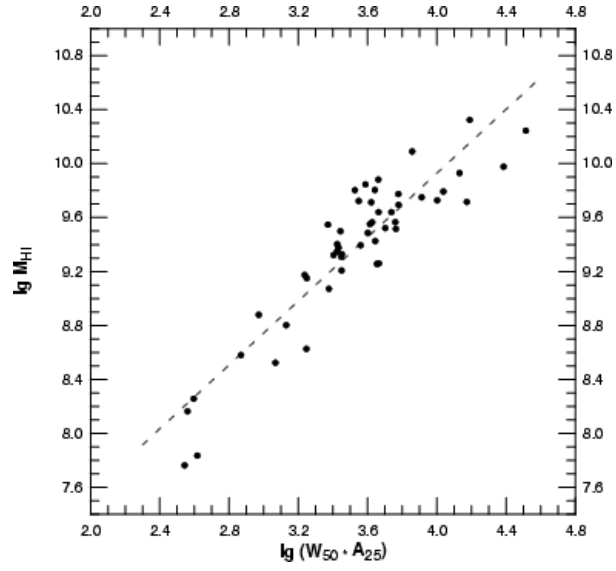


Figure 7: HI mass versus specific angular momentum